ARTICLE

Analysis of the Influence of Cell Heterogeneity on Nanoparticle Dose Response

Matthew J. Ware,[†,‡] Biana Godin,[‡] Neenu Singh,[†] Ravish Majithia,[§] Sabeel Shamsudeen,[†,‡] Rita E. Serda,[†,‡,§] Kenith E. Meissner,[∥] Paul Rees,[†,⊥] and Huw D. Summers[†,*]

[†]Centre for Nanohealth, College of Engineering and College of Medicine, Swansea University, Swansea SA2 8PP, U.K., [‡]Department of Nanomedicine, Houston Methodist Research Institute, Houston, Texas 77030, United States, [§]Department of Surgery, Baylor College of Medicine, 6501 Fannin Street, Houston, Texas 77030, United States, [∥]Department of Biomedical Engineering, Texas A&M University, College Station, Texas 77843, United States, and [⊥]Broad Institute of MIT and Harvard, Cambridge, Boston, Massachusetts 02148, United States

ABSTRACT Understanding the effect of variability in the interaction of individual cells with nanoparticles on the overall response of the cell population to a nanoagent is a fundamental challenge in bionanotechnology. Here, we show that the technique of time-resolved, high-throughput microscopy can be used in this endeavor. Mass measurement with single-cell resolution provides statistically robust assessments of cell heterogeneity, while the addition of a temporal element allows assessment of separate processes leading to deconvolution of the effects of particle supply and biological response. We provide a specific demonstration of the approach, *in vitro*, through time-resolved measurement of fibroblast cell (HFF-1) death caused by exposure to cationic nanoparticles. The results show that heterogeneity in cell area is the major source of variability with area-dependent nanoparticle capture rates determining the time of cell death and hence the form of the exposure–response characteristic. Moreover, due to the particulate nature of the nanoparticle suspension, there is a reduction in the particle concentration over the course of the experiment, eventually causing saturation in the level of measured biological outcome. A generalized mathematical description of the system is proposed, based on a simple model of particle depletion from a finite supply reservoir. This captures the essential aspects of the nanoparticle–cell interaction dynamics and accurately predicts the population exposure–response curves from individual cell heterogeneity distributions.

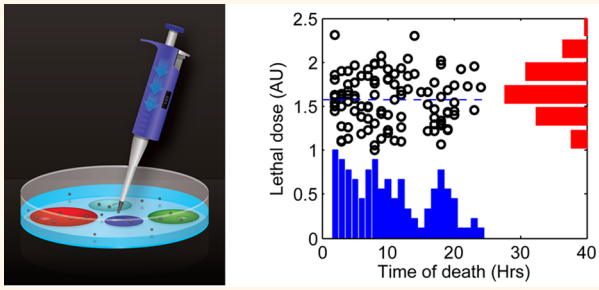

KEYWORDS: nanomedicine · nanotoxicology · bionanotechnology · nanoparticle dose · nanoparticle exposure · dose–response characteristic · high-throughput microscopy

The role of variability at the single-cell level in determining population-wide biological response is a topic of much current interest.[1−3] The advent of high-throughput microscopy has provided the technology with which individual cells can be studied en masse and their interrelations, which define population level traits, understood.[4] Within the field of bionanotechnology, the development of a plethora of nanoparticles and their testing in biological assays has led to widespread appreciation of the unique properties present at the nanoscale and the need to reassess standard metrics when it comes to nanoparticle–cell interactions.[5−7] However, much of this work is focused on population-averaged measurements such as dose–response curves, and despite intensive efforts over a decade or more, robust, standardized protocols are still not available.[8] Knowledge of the source and form of variation in biological responses to nanoparticles is an obvious requirement if we are to gain a detailed understanding in areas such as nanomedicine[9−11] and nanotoxicology,[12,13] where the level of drug or toxin determines the biological output, namely therapeutic outcome or mortality level. Beyond these areas, the impact of variations in cell response is still important; for example, it is critical in determining the level of reporter signal from intracellular nanosensors.[14,15] A reliance on population-averaged measures which ignore cell-to-cell variability is also prevalent in wider pharmacological studies. A single identifying parameter, z, is widely used in drug-screening

* Address correspondence to h.d.summers@swansea.ac.uk.

Received for review January 10, 2014 and accepted June 12, 2014.

Published online June 13, 2014
10.1021/nn502356f

assays; this is based on measurement of mean values across a cell population and an imposed assumption of a Gaussian distribution profile for assessed metric. Approaches of this type are inherently limited for describing cellular heterogeneity.[16]

There is now a comprehensive body of work reporting on *in vitro* studies in which the complexities of the processes through which particles arrive at the cell membrane and interact with it (e.g., diffusion and sedimentation) have been explored in detail.[17−19] Likewise, it is known that agglomeration of the particles, which is dependent on media content and the functional coating on the particles, can also alter cellular uptake.[20] Given the complexity and multiplicity of nanoparticle−cell interactions and their relation to toxic effects within the cell,[21,22] we present a simplifying approach that aims to describe the dose response in terms of a dose metric relating to particle uptake (proportional to internalized dose rather than exposure) and a response, captured as a complete description across the varying susceptibility of the cell population. In a typical dose−response experiment, the summed response of a cell population to a range of exposure concentration is measured. In this case, the assay outcome is determined by a convolution of the particle supply and uptake dynamics, which determine the relation of exposure level to accumulated cellular dose and the heterogeneity in cell response to this dose. Thus, the innate biological susceptibility is not directly apparent. However, through the adoption of time-resolved approaches the evolution of biological response, as an increasing dose elicits a reaction from evermore resistant cells, can be tracked.[23] Importantly, the study of the response over increasing time intervals as opposed to increasing exposure concentrations allows deconvolution of supply processes and response mechanisms and hence separation of a response that is due to a limitation in the toxin or drug supply from that due to an innate resistance in the cell population. We demonstrate the application of this approach using cationic nanoparticles (polyethyleniminecoated quantum dots: PEI-QD) to induce death in *in vitro* cultured HFF-1, fibroblasts. The collection of time−mortality data allows us to quantify the time-dependent nanoparticle supply and thus transform the known exposure concentrations to a measure of accumulated particle dose within the cells. We deliberately concentrate on the internalized dose, *i.e.*, we measure the nanoparticle dose actually delivered to the cell. By adopting this approach, we avoid the complications which arise when trying to describe the particle delivery due to the complexities of agglomeration, sedimentation, and diffusion dynamics in solution. From this "global" dose−response metric we use individual cell responses to deconvolve uptake variability and so extract the innate cellular susceptibility to membrane disruption by the charged nanoparticles.

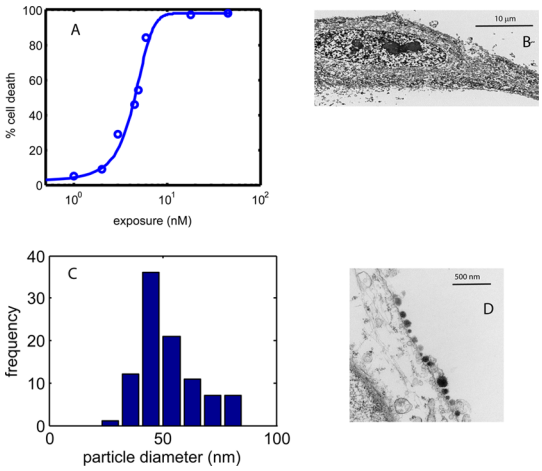

Figure 1. (A) Exposure−response curve for HFF-1 cells exposed to PEI-QDs for a 24 h duration. Data was collected from 81 image frames encompassing >4000 cells. (B) Electron micrograph of a cell section showing severe membrane disruption due to the high cationic charge of the PEI-QDs. (C) Size distribution of PEI-QDs at the cell surface measured from electron microscopy images (*n* = 93). (D) Electron micrograph of a cell section showing individual PEI-QDs on the cell membrane.

RESULTS AND DISCUSSION

Standard End-Point Concentration−Response Measurement. The exposure−response curve measured after 24 h exposure of fibroblasts to a range of PEI-QD concentrations is shown in Figure 1A. This displays the classic sigmoid curve of increasing cell mortality in response to the nanoparticle concentration in the medium.[24] In this case, the highly charged, PEI-coated, CdSe quantum dots (PEI-QDs) cause death through disruption of cellular membranes,[25] an example of which is shown in Figure 1B (see the Supporting Information for further information). Electron microscopy analysis of the size distribution of the particles which interact with the cell membrane is shown in Figure 1C. Individual particles with a size range of 30−80 nm can be seen attached to the cell surface in the electron micrograph of Figure 1D.

Long-term studies of cytotoxicity of Cd-containing QDs generally attribute cytotoxicity to a Cd^{2+} leakage from the core.[26] However, in our study, all the experiments were done within a 24 h time period, and the chemical stability of Cd-based quantum dots, at nanomolar concentrations, over this time frame is well documented.[27] We are confident, therefore, that the surface chemistry of the particles is the dominant factor determining the effects observed. The literature on the toxic effect of amine-modified particles on cells highlights lipid membrane disruption as a key determinant,[25] and our TEM micrographs (see the Supporting Information) confirm significant membrane damage at 3 and 24 h following PEI-QD exposure. This corresponds well with DRAQ7 signals that are seen within minutes of exposure at particular concentrations of PEI-QDs and which are due to membrane permeabilisation.

Measurements such as those presented in Figure 1 provide a quantitative benchmark for standardization and comparison of different studies; however their power to inform on underlying biological processes is limited as they only provide end-point information on the mean response of a population of cells. For example, the data in Figure 1 shows that on average 50% of cells die within 24 h when exposed to a 4.5 nM concentration of PEI-QDs. While this defines the LD_{50} point the cause of the observed cell mortality is still obscure; do 50% of the population remain alive because they are resilient and able to withstand the effects induced by the nanoparticles or because they have acquired a lower particle dose? The metric is unable to distinguish between supply and response variation and so cannot help in answering this question.

Time-Dependent Exposure–Response Measurement. In a typical *in vitro* experiment, the cell population is exposed to a known solution particle concentration, C, of nanoparticles, for a fixed time, t. The total available number of nanoparticles administered to the culture media is then, $n_0 = CV$, where V is the volume of solution. In traditional dose–response studies of chemical agents or biological pathogens the dose delivered is assumed to be a linear function of time, described by an average arrival rate, λ, per particle. Using this approach, the number of particles or dose taken up by a cell population, $n_{dose}(t) = CV\lambda t$. If the cell response is proportional to this particle dose then it follows Haber's rule;[27] *i.e.*, it is a function of the product of concentration and duration of exposure. In dose–response theory, the variability of the cell response is included using a probability distribution function (PDF) of cell susceptibility parametrized by a mean number, μ, of particles to elicit a response (with standard deviation, σ). The cumulative frequency of this probability distribution (CDF) charts the dose–response curve,[28] the summed response of the cell population as the particle dose increases. Assuming a normal distribution for the susceptibility PDF, the time-dependent response curve due to nanoparticle accumulation is given by

$$R(t) = \int_{-\infty}^{n_{dose}(t)} \frac{1}{\sqrt{2\pi\sigma^2}} \exp^{-\left(\frac{n-\mu}{\sqrt{2\sigma^2}}\right)^2} dn$$

$$= \frac{1}{2}\left[1 + \mathrm{erf}\left(\frac{n_{dose}(t) - \mu}{\sqrt{2\sigma^2}}\right)\right] \quad (1)$$

Thus, measurement of the time-differentiated cellular response, $dR(t)/dt$ can provide the cell susceptibility distribution.

Time–mortality curves for the HFF-1 cells over a range of PEI-QD exposures of 0–24 h duration are shown in Figure 2. For the 18 nM exposure concentration the supply of particles is such that even the most resistant cells acquire a lethal dose. At lower exposure concentrations the % cell death plateaus well before the 24 h point, and extrapolation of the data indicates that low susceptibility cells are unlikely to reach the required particle dose threshold for cell death. Interpreting these results in terms of eq 1: the saturation in % cell death at later times is due to diminishing increments in the integration across the susceptibility PDF as the value of n_{dose} no longer linearly increases with time; i.e., there is a limitation to particle supply.

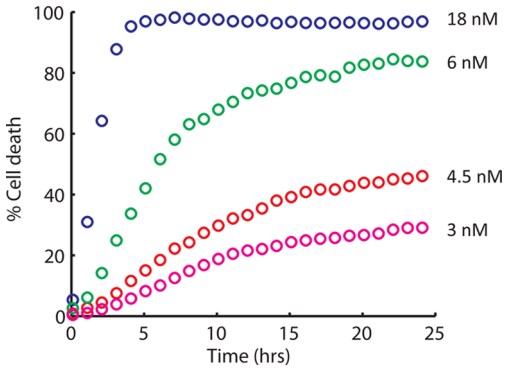

Figure 2. Time–mortality curves for HFF-1 cells exposed to PEI-QDs, at varying concentrations, over a 24 h period. Data were collected from 81 image frames encompassing >3000 cells.

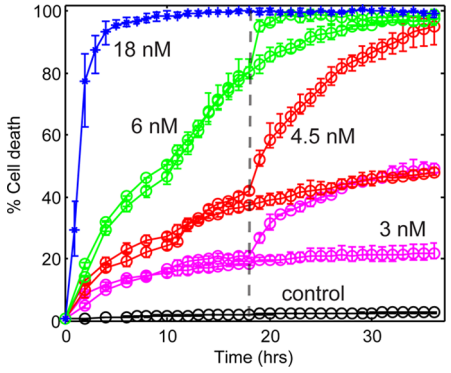

Figure 3. Time–mortality curves for HFF-1 cells exposed to PEI-QDs with replenishment of culture medium after 18 h (indicated by dashed gray line). For $t > 18$ h the two curves at each exposure concentration plot the % cell death with (higher values) and without (lower values) replenishment of the medium.

Particle Supply from a Fixed Reservoir. To confirm that the limitation in levels of cell death is caused by limited nanoparticle availability, we repeated the time–mortality assay with an added replenishment step. After 18 h of exposure, the medium containing nanoparticles was removed and fresh medium (of identical volume and with the same particle concentration) was introduced for the remainder of the assay. The results, shown in Figure 3, clearly highlight the effect of supply depletion as the renewal of particle supply produces an immediate increase in cell death. Similarly, experiments at fixed concentration but increasing exposure solution volumes also produced increased values of % cell death due to greater number of particles

(see Supporting Information). It is clear that in these experiments there is nonlinear particle accumulation over time and so Haber's rule is not applicable. Saturation of the number of particles internalized by cells is a common observation in nanoparticle uptake experiments. If the internalization mechanism is receptor mediated endocytosis, then this phenomenon can occur due to limitation of the available receptors during the course of the experiment.[29] However, in our experiments, in which unspecific cell death occurs due to accumulation of particles at the membrane, it is limitation in particle supply which leads to dose saturation. This is confirmed by measurements of particle accumulation onto the bare surface of the culture dish, which show the same saturation of fluorescence signal (see the Supporting Information). The problem of particle depletion is particularly acute in nanoparticle assays because loading over a few hours leads to a total accumulated dose in the picomole range (10^5–10^7 particles per cell in $\sim 10^6$ cells[30−33]). Typically, in exposure volumes of mL at nM concentrations (picomole quantities) a major fraction of available particles are therefore removed from solution, and hence, depletion of particle supply will be a common occurrence.

The time dependence of toxicity has been well studied within *in vivo* settings,[34] especially within ecological toxicity assessement.[35] In general, the accumulation of small-molecule drugs is characterized by a two-way flow, in and out of the cell,[36] as molecules can diffuse across the membrane according to the direction of the concentration gradient or are actively removed from the cell by molecular efflux pumps.[37] This is in contrast to the general situation when using nanoparticles, where cellular accumulation is in effect a one-way valve. Nanoparticles are internalized by endocytic processes and encapsulated in membrane-bound vesicles, and while there is some exocytosis,[38] this is limited and the general trend is for long-term accumulation of particles.[39]

Extraction of a Global Exposure−Response Metric. To mathematically describe the nonlinear particle supply, we consider the cellular accumulation of particles from a fixed initial reservoir (the initial exposure number, n_0), assuming that the accumulation rate is proportional to the remaining number of available particles, $n_0 - n_{dose}$ (see the Supporting Information for full details). This provides a simple expression for the total accumulated particle number across the cell population

$$n_{dose}(t) = \eta C V (1 - e^{-t/\tau}) \qquad (2)$$

where η is a constant describing the capture cross-section of cells, *i.e.*, it accounts for the fraction of particles that attach to cells rather than to the culture well surface. The parameter τ is the average accumulation time per particle, is constant with respect to t and n_{dose}, and is determined by the multiplicity of supply

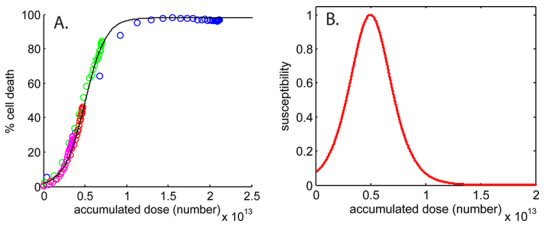

Figure 4. (A) Percent cell death as a function of total accumulated dose in the cell population for 3 (magenta symbols), 4.5 (red), 6 (green), and 18 nM (blue) exposure concentrations. (B) Cell population susceptibility distribution obtained by differentiation of the dose−response curve in (A).

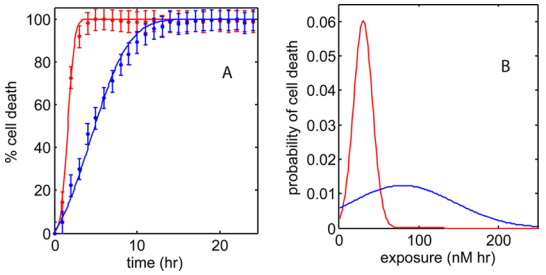

Figure 5. (A) Percent cell death as a function of time for HFF-1 cells (blue) and primary fibroblasts (red) exposed to an 18 nM concentration of PEI-QDs. (B) Cell population susceptibility distribution obtained by differentiation of the time−response curves in (A).

side mechanisms, *e.g.*, diffusion, sedimentation, and agglomeration. In effect, τ provides a single metric describing the average behavior of the particle dispersion and allows us to simplify the description of dose accumulation. Given that the experimental measure to which eq 2 is compared is an internalized dose (*i.e.*, we measure the outcome rather than the mechanisms of particle supply), this parametrization of the particle dynamics is a valid approach. Using eq 2, the time and concentration dependence of cellular response seen in Figure 2 can be transformed to show % cell death as a function of accumulated dose. This is shown in Figure 4A for a τ value of 5.5 h; in this case, η is assumed to be ~ 1 due to the high cell confluency. As the cell response is now plotted as a function of accumulated dose it is independent of the route to this accumulation; thus, the profile is a "global" measure, unaffected by the intricacies of particle supply.

The shape of the response curve is now determined solely by the biological susceptibility to the nanoparticles, and thus, its differential provides the susceptibility probability distribution of the population (Figure 4B); *i.e.*, it describes the population-averaged vulnerability of the cells. We demonstrate the utility of this link between response curve and cell susceptibility through a study of the toxicity of the PEI-QDs in primary and immortalized fibroblasts. Figure 5A shows the measured cell death over a 24 h period for the HFF-1 cells and for a population of primary human

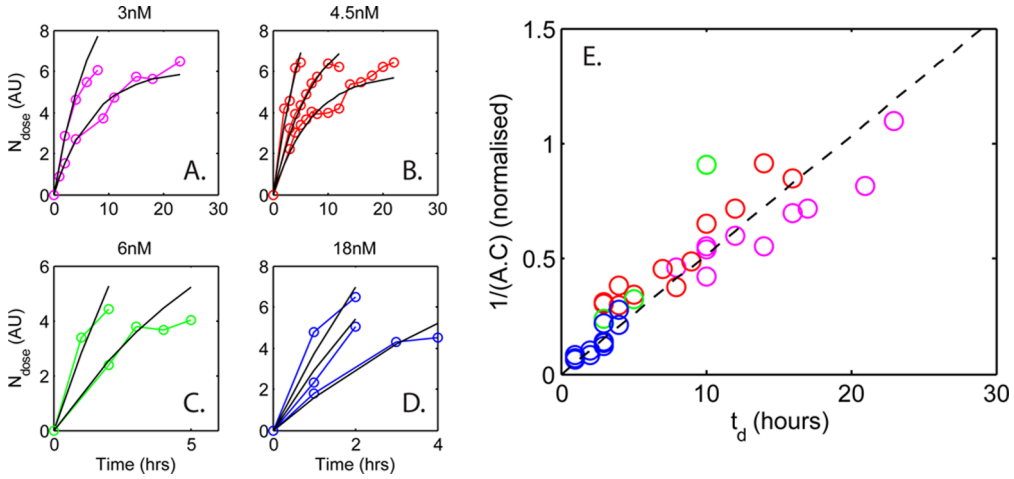

Figure 6. Time dependence of relative particle dose in individual cells obtained from measurement of total fluorescence per cell for exposure concentrations of (A) 3, (B) 4.5, (C) 6, and (D) 18 nM; solid black lines indicate model fits (using eq 2). (E) Correlation plot of inverse cell area × concentration versus time of cell death, t_d (colors used for different exposure concentrations as per Figure 5A–D).

dermal fibroblasts. There is a clear increase in cell death in the primary population at a given time. An enhanced susceptibility of primary derived cells to cationic particles has been well documented and is related to the increased mitochondrial activity in these cells compared to immortalized cell lines.[40,41] Here, we are able to quantify this difference in toxicity by extracting the susceptibility distribution directly from the temporal dose response curve (Figure 5B). This indicates a mean susceptibility of 32 nM h for primary cells compared to 85 nM h for the HFF-1 cells with associated variance of 40% and 82%, respectively. Thus, primary cells display a more homogeneous as well as an enhanced susceptibility to the PEI-QDs. In this example, the ability to extract the innate biological susceptibility leads to a clear indication of different biological mechanisms driving the response of primary and immortalized cells. This stems from "the Warburg effect", which describes the altered metabolism of cancer cells leading to increased reliance on aerobic glycolysis rather than mitochondrial oxidative phosphorylation to generate the energy needed for cellular processes.[42] The data in Figure 5B provides a quantification of the increased tolerance of immortalized cells to cationic particles, produced by this reduced reliance on mitochondrial processes.

Susceptibility of Individual Cells. The biological susceptibility profile shown in Figure 4B is obtained from population wide measurement of the fraction of cells which respond at each dose value and is based on a calculation of the total accumulated dose, across all cells ($n > 4000$). To understand the role of individual cell heterogeneity in determining this population response, we use high-throughput microscopy to directly analyze cell-to-cell variability in dose and response. The time dependence of dose accumulation in single cells was tracked up to the point of cell death by surrogate measurement of the total QD fluorescence. Representative data from nine individual cells chosen from the measured population of over 4000, exposed to a range of PEI-QD concentrations, are shown in Figure 6A–D. Two general points can be made from inspection of these data: (i) there is a "threshold" dose range at which the accumulated particle dose is sufficient to trigger cell death; (ii) the rate of particle accumulation in individual cells varies greatly for the same exposure concentration and it is this variable dose accumulation which primarily determines the time of death.

Equation 2 indicates that the total acquired dose is dependent upon the cross-sectional area available for nanoparticle capture, as described by the parameter η. At the single-cell level, this implies a cell-area dependent dose with larger cells possessing a larger capture cross-section and hence accumulating particles more rapidly. To assess the validity of this hypothesis, we plotted the predicted dose accumulation for individual cells based on eq 2 (Figure 6A–D), where for single cells $\eta = A_{cell}/A_{well}$. The cell area (A_{cell}) was obtained from the microscopy images, and the value of τ was set to 5.5 h as indicated by the data in Figure 4. There is close agreement of the data with eq 2 strongly corroborating the hypothesis of a cell area dependent uptake. The clear correlation in the time of cell death, t_d to the inverse of cell area is shown in Figure 6E (Pearson correlation index = 0.92).

The plots in Figure 6A–D display two independent sources of heterogeneity in cell–nanoparticle interaction dynamics. There is variability in the acquired dose at a fixed time point due to the cell area dependent accumulation (dose heterogeneity) and there is an innate variability in the ability of individual cells to survive a given dose (response heterogeneity). To assess the relative importance of these we plot the QD dose which triggers cell death versus the time of

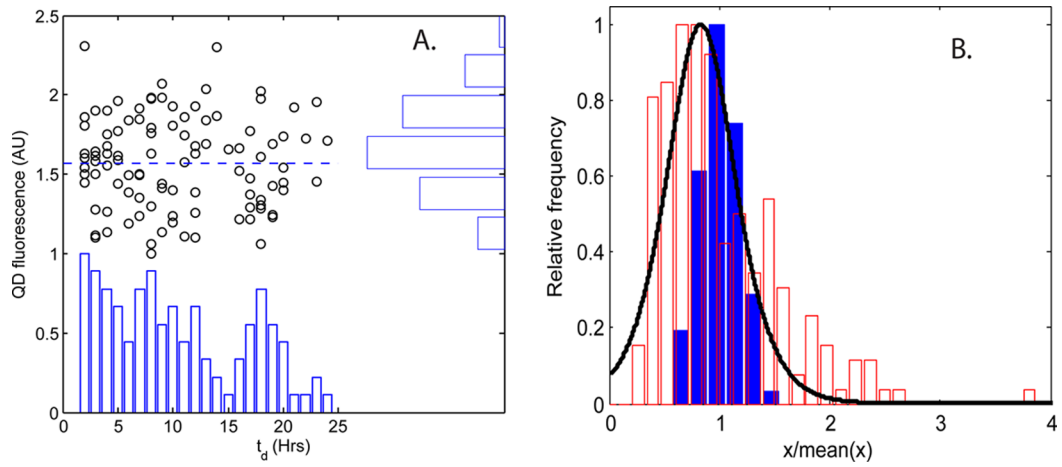

Figure 7. (A) Dot plot of time of cell death and the QD fluorescence (surrogate for particle dose) at that time ($n = 89$). The data are also shown in histogram form with the horizontal dashed line indicating the mean fluorescence at time of death. (B) Normalized histograms of population susceptibility (black line), cell area (red bars), and dose at threshold (blue bars).

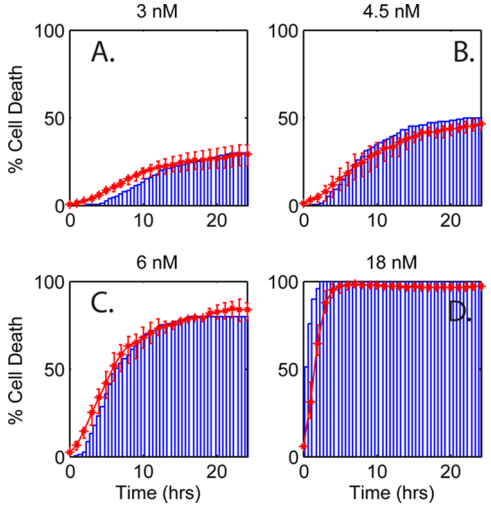

Figure 8. Measured (red curve) and predicted (blue bars) time–mortality curves for HFF-1 cells exposed to PEI-QDs at (A) 3, (B) 4.5, (C) 6, and (D) 18 nM concentrations. Predicted values based on measured cell area distribution and eqs 2 and 3.

death (Figure 7A, n = 89). The dose and response heterogeneities are represented in Figure 7A by histograms of time of death and dose at death, respectively. Having quantified the cellular heterogeneity distributions we compare them in Figure 7B to the population distribution of Figure 4B. The comparison is made using a normalized histogram variable of x/mean(x) to allow assessment of the relative variance of the profiles and clearly shows that it is the cell area variability which is the dominant factor in determining the population level characteristic. (For a mathematical assessment of the role of these sources of heterogeneity, see the Supporting Information.)

Relating Individual Cell and Population Traits. Having established the primary driver of cell response at the individual cell level, this information can be used to construct a complete model of cell-nanoparticle interaction with an *ab initio* description of the population response based on single cell studies. To do this, we use the measured cell area heterogeneity ($n = 700$) and mean dose at death, n_{th} (indicated in Figure 7A) to calculate the distribution in time of death, t_d, using a reformulation of eq 2:

$$t_d = \tau \ln\left[1 - \frac{n_{th}}{CV}\frac{A_{well}}{A_{cell}}\right]^{-1} \quad (3)$$

Cumulative integration of the t_d distribution across a time interval t then provides a predicted value of the % cell death at t. The results of this analysis are presented in Figure 8 together with the directly measured experimental data (replotted from Figure 2). The model is thus completely defined by experimentally determined parameters and its validity confirmed by the close match of the simulation to the data over a wide range of exposure concentration and duration.

CONCLUSIONS

In summary, we have used high-throughput microscopy to understand the link between individual cells and the population wide response to nanoparticles. This allows deconstruction of the standard exposure–response metric to separate the roles of particle supply and biological response and highlights the sources of cell heterogeneity which lead to response variability. While we demonstrate this approach using fluorescent, quantum dots the mathematical formulism which we present is ultimately used to predict the time dependence of cell death; thus in this respect it is independent of the type of nanoparticle used and hence has wide applicability. Tools such as this are important for future studies in the fields of nanomedicine and nanotoxicology to aid in the progression from description of nanoparticle interactions

to quantification of the biological processes and mechanisms that underpin them. In certain subfields such as cancer therapeutics[43] and genotoxicity,[44] the ability to understand individual cell response rather than the population average is essential as the "rare" cell can dictate the end result.

METHODS

Materials, Cell Culture, and Cell Lines. Human foreskin fibroblast cells (HFF-1, ATCC SCRC-1041) and primary human dermal fibroblasts were obtained from the American type culture collection (ATCC, Manassas, VA). The HFF-1 cells were cultured (37 °C; 5% CO2) in DMEM medium supplemented with 15% fetal bovine serum (FBS), 4 mM L-glutamine, 1 mM sodium pyruvate, and 1% penicillin (50 IU/mL)/streptomycin (50 μg/mL). The primary fibroblasts were cultured in fibroblast basal medium supplemented with a low serum growth kit containing 2% serum (ATCC). Cells were grown in 75 cm^2 flasks placed in a humidified incubator at 37 °C with 5% CO2 before use. Quantum dots (QDs) with a CdSe core and a ZnS shell synthesized in a coordinating solvent tri-*n*-octylphosphine oxide (TOPO, 99%, Aldrich) in accordance with previously published procedures.[45] The QDs were synthesized in a single-mode CEM Discover microwave reactor operating at 300 W, 2.45 GHz. Cadmium oxide (CdO, 99.99%, Alfa Aesar, 0.0514 g, 0.4 mM) along with tetradecylphosphonic acid (TDPA, 98%, Alfa Aesar, 0.2232 g, 0.8 mM) and TOPO (3.7768 g, 9 mM) were heated with continuous stirring in a 125 mL glass flask. The solution was heated for 15 min at approximately 300 °C under argon (Ar) flow. A selenium stock solution (Aldrich, 99%, 0.0411 g, 0.5 mM) dissolved in 2.4 mL (2 g) of tri-*n*-octylphosphine (TOP, 99%, Aldrich) was injected at 270 °C, and Q-Dots were allowed to grow for 150 s. A ZnS shell was grown on the CdSe cores by injecting a mixture of Zn and S precursors: 1.6 mL (12 mM) of dimethylzinc (DMZ-1 M in heptane, Aldrich), 0.42 mL (2 mM) of hexamethyldisilathiane (HMDS, Aldrich), and 6.3 mL (14 mM) of TOP. The reaction mixture was heated for 30 min at 200 °C. The quantum yield of the Q-Dots increased on annealing the particles at a temperature of 100 °C for a period of 2 h.

The QDs were surface modified with high molecular weight branched polyethylenimine (BrPEI) (Aldrich, MW 25000). Briefly, a 10 mg/mL solution of BrPEI in chloroform was mixed with an equal volume of 2−4 μM QDs. The mixture, kept at room temperature, was tumbled overnight. PEI-QDs were precipitated from the mixture by addition of excess cyclohexane (Sigma-Aldrich, 0.99%) and suspended in deionized water. Excess BrPEI was extracted from the aqueous QDs solution by addition of fresh chloroform, which was phase-separated from water.

The zeta potential and the hydrodynamic diameter of the PEI-QDs when suspended in phosphate buffer (PB) at a concentration of 21 nM was measured using a Zetasizer Nano ZS (Malvern Corp, Worcestershire, UK) using a 633 nm laser. The PEI-QD diameter was also measured from scanning electron micrographs, performed when the PEI-QDs at a concentration of 3 nM were suspended in 2 mL of DMEM cell culture media and 15% FBS and supplemented with 1% penicillin G/streptomycin. The zeta potential and the hydrodynamic diameter of the PEI-QDs when suspended in phosphate buffer were measured at +18.6 ± 5.67 mV and 27.68 ± 5.67 nm, respectively, and the PEI-QDs a mean diameter of 51.39 ± 17.30 nm when measured from scanning electron micrographs.

Cytotoxicity Analysis. Cytotoxicity was quantified using DRAQ7 (Biostatus Ltd., UK) staining, which is a far-red fluorescent necrotic dye which was kindly gifted by Biostatus Ltd. DRAQ7 is excluded from viable cells and, hence, only stains the nuclei in dead and/or cell membrane permeabilized cells as it passively diffuses through the damaged cytoplasmic and nuclear membranes and eventually binds with A−T-rich repeats in DNA.

HFF-1 cells were seeded at a concentration of 70000 cells per well in Greiner Bio One Cellstar tissue culture six-well plate for 24 h. The PEI QDs were vortexed for 5 s, and 2, 3, 4.5, 6, or 18 nM concentrations of PEI-QDs and 3 μM concentration of DRAQ7 were placed in 2 mL of complete DMEM medium. The cells were washed twice in serum-free medium and incubated with 2 mL of complete DMEM medium containing PEI QDs and DRAQ7. High-throughput, time-lapse-based experiments were performed within 5−10 min of dosing using the In-Cell Analyzer 2000 microscope (GE Healthcare, UK). Images were obtained hourly for 24 h from 81 fields with each field containing approximately 40−50 cells, meaning a total of over 4000 cells were imaged at each time point. Cells were imaged at 20× magnification in three channels: the DRAQ7 and the PEI-QDs in fluorescence mode with excitation/emission wavelengths of 633/655 nm and 350/568 nm, respectively. Brightfield images were also obtained using transmitted white light. At the end of the time lapse experiments, the cells were dosed with 10 μM PEI-QDs in 2 mL of media with 0.5 h exposure, which caused 100% cell death in each well. An additional set of images was collected from which a measure of the total number of cells in each well was obtained. Cell death was quantified by the automated measure of the DRAQ7signals at each time point using In-Cell Developer Toolbox software (GE Healthcare, UK) and was displayed as a percentage of the total cells within each well. In addition to this, a separate time lapse was performed from 0 to 43 h to confirm the stability of the DRAQ7 signals between 0 and 43 h.

Conflict of Interest: The authors declare no competing financial interest.

Supporting Information Available: Electron microscopy images of particle accumulation on the cell membrane, time−mortality study with increasing volume of medium, time-resolved fluorescence accumulation at the culture well surface, and mathematical descriptions of time dependent particle dose and of cell heterogeneity distributions. This material is available free of charge *via* the Internet at http://pubs.acs.org.

Acknowledgment. We acknowledge the Swansea University and Houston Methodist Research Institute Joint Ph.D. Graduate Program. We also acknowledge the support of the TMHRI Advanced Cellular and Tissue Microscope Core Facility where time lapse imaging was performed.

REFERENCES AND NOTES

1. Niepel, M.; Spencer, S.; Sorger, P. Non-Genetic Cell-to-Cell Variability and the Consequences for Pharmacology. *Curr. Opin. Chem. Biol.* **2009**, *13*, 556–561.
2. Altschuler, S. J.; Wu, L. F. Cellular Heterogeneity: Do Differences Make a Difference? *Cell* **2010**, *141*, 559–563.
3. Snijder, B.; Pelkmans, L. Origins of Regulated Cell-to-Cell Variability. *Nat. Rev. Mol. Cell Biol.* **2011**, *12*, 119–125.
4. Snijder, B.; Sacher, R.; Rämö, P.; Damm, E. M.; Liberali, P.; Pelkmans, L. Population Context Determines Cell-to-Cell Variability in Endocytosis and Virus Infection. *Nature* **2009**, *461*, 520–523.
5. Chithrani, B. D.; Ghazani, A. A.; Chan, W. C. W. Determining the Size and Shape Dependence of Gold Nanoparticle Uptake into Mammalian Cells. *Nano Lett.* **2006**, *6*, 662–668.
6. Hardman, R. A. Toxicological Review of Quantum Dots: Toxicity Depends on Physiochemical and Environmental Factors. *Environ. Health Perspect.* **2005**, *1142*, 165–172.
7. Nell, A. E.; Mädler, L.; Velegol, D.; Xia, T.; Hoek, E. M. V.; Somasundaran, P.; Klaessig, F.; Castranova, V.; Thompson, M. Understanding Biophysicochemical Interactions at the Nano−Bio Interface. *Nat. Mater.* **2009**, *8*, 543–557.
8. Editorial: 'Join the Dialogue'. *Nat. Nanotechnol.*, **2012**, *7*, 545−546.
9. Hillaireau, H.; Couvreur, P. Nanocarriers' Entry into the Cell: Relevance to Drug Delivery. *Cell. Mol. Life Sci.* **2009**, *66*, 2873–2896.

10. Scheinberg, D. A.; Villa, C. H.; Escorcia, F. E.; McDevitt, M. R. Conscripts of the Infinite Armada: Systematic Cancer Therapy Using Nanomaterials. *Nat. Rev. Clin. Oncol.* **2010**, *7*, 266–276.
11. Koo, O. M.; Rubinstein, I.; Onyuksel, H. Role of Nanotechnology in Targeted Drug Delivery and Imaging: A Concise Review. *Nanomedicine* **2005**, *1*, 193–212.
12. Oberdörster, G.; Maynard, A.; Donaldson, K.; Castranova, V.; Fitzpatrick, J.; Ausman, K.; Carter, J.; Karn, B.; Kreyling, W.; Lai, D.; et al. Principles for Characterizing the Potential Human Health Effects from Exposure to Nanomaterials: Elements of a Screening Strategy. *Part. Fibre Toxicol.* **2005**, *2*, 1–35.
13. Nel, A.; Xia, T.; Mädler, L.; Li, N. Toxic Potential of Materials at the Nanolevel. *Science* **2006**, *311*, 622–627.
14. Lartigue, L.; Wilhelm, C.; Servais, J.; Factor, C.; Dencausse, A.; Bacri, J.-C.; Luciani, N.; Gazeau, F. Nanomagnetic Sensing of Blood Plasma Protein Interactions with Iron Oxide Nanoparticles: Impact on Macrophage Uptake. *ACS Nano* **2012**, *6*, 2665–2678.
15. Clarke, S. J.; Hollmann, C. A.; Zhang, Z.; Suffern, D.; Bradforth, S. E.; Dimitrijevic, N. M.; Minarik, W. G.; Nadeau, J. L. Photophysics of Dopamine-Modified Quantum Dots and Effects on Biological Systems. *Nat. Mater.* **2006**, *5*, 409–417.
16. Singh, S.; Carpenter, A. E.; Genovesio, A. Increasing the Content of High-Content Screening: An Overview. *J. Biomol. Screening* **2014**, *19*, 640–650.
17. Hinderliter, P. M.; Minard, K. R.; Orr, G.; Chrisler, W. B.; Thrall, B. D.; Pounds, J. G.; Teeguarden, J. G. ISDD: A Computational Model of Particle Sedimentation, Diffusion and Target Cell Dosimetry for *In Vitro* Toxicity Studies. *Part. Fibre Toxicol.* **2010**, *7*, 36.
18. Wittmaack, K. Excessive Delivery of Nanostructured Matter to Submersed Cells Caused by Rapid Gravitational Settling. *ACS Nano* **2011**, *5*, 3766–3778.
19. Teeguarden, J. G.; Hinderliter, P. M.; Orr, G.; Thrall, B. D.; Pounds, J. G. Particokinetics *In Vitro*; Dosimetry Considerations for *In Vitro* Nanoparticle Toxicity Assessments. *Toxicol. Sci.* **2007**, *95*, 300–312.
20. Lesniak, A.; Fenaroli, F.; Monopoli, M. P.; Åberg, C.; Dawson, K. A.; Salvati, A. Effects of the Presence or Absence of a Protein Corona on Silica Nanoparticle Uptake and Impact on Cells. *ACS Nano* **2012**, *6*, 5845–5857.
21. Rivera-Gil, P.; De Aberasturi, D. J.; Wulf, V.; Pelaz, B.; Del Pino, P.; Zhao, Y.; De La Fuente, J. M.; De Larramendi, I. R.; Rojo, T.; Liang, X.; et al. The Challenge to Relate the Physicochemical Properties of Colloidal Nanoparticles to Their Cytotoxicity. *Acc. Chem. Res.* **2013**, *46*, 743–749.
22. Cho, E. C.; Zhang, Y.; Cai, X.; Moran, C. M.; Wang, L. V.; Xia, Y. A Quantitative Analysis of the Fate of Au Nanocages after Uptake by U87-MG Tumor Cells Under Both *in Vitro* and *in Vivo* Conditions. *Angew. Chem.* **2013**, *52*, 1152–1155.
23. Bliss, C. I. The Calculation of the Time–Mortality Curve. *Ann. Appl. Biol.* **1937**, *24*, 815–852.
24. Bliss, C. I. The Calculation of the Dosage–Mortality Curve. *Ann. Appl. Biol.* **1935**, *22*, 134–167.
25. Mecke, A.; Majoros, I. J.; Patri, A. K.; Baker, J. R., Jr.; Holl, M. M.; Orr, B. G. Lipid Bilayer Disruption by Polycationic Polymers: The Roles of Size and Chemical Functional Group. *Langmuir* **2005**, *21*, 10348–10354.
26. Su, Y.; He, Y.; Lu, H.; Sai, L.; Li, Q.; Li, W.; Wang, L.; Shen, P.; Huang, Q.; Fan, C. The Cytotoxicity of Cadmium Based, Aqueous Phase – Synthesized, Quantum Dots and its Modulation by Surface Coating. *Biomaterials* **2009**, *30*, 19–25.
27. Gaylor, D. W. The Use of Haber's Law in Standard Setting and Risk Assessment. *Toxicology* **2000**, *14*, 17–19.
28. Haas, C. N. Conditional Dose-Response Relationships for Microorganisms: Development and Application. *Risk Anal.* **2002**, *22*, 455–463.
29. Lunov, O.; Zablotskii, V.; Syrovets, T.; Röcker, C.; Tron, K.; Nienhaus, G. U.; Simmet, T. Modeling Receptor-Mediated Endocytosis of Polymer-Functionalized Iron Oxide Nanoparticles by Human Macrophages. *Biomaterials* **2011**, *32*, 547–555.
30. Summers, H. D.; Brown, M. R.; Holton, M. D.; Tonkin, J. A.; Hondow, N.; Brown, A. P.; Brydson, R.; Rees, P. Quantification of Nanoparticle Dose and Vesicular Inheritance in Proliferating Cells. *ACS Nano* **2013**, *7*, 6129–6137.
31. Krpetić, Z.; Saleemi, S.; Prior, I. A.; Sée, V.; Qureshi, R.; Brust, M. Negotiation of Intracellular Membrane Barriers by TAT-Modified Gold Nanoparticles. *ACS Nano* **2011**, *5*, 5195–5201.
32. Wilhelm, C.; Gazeau, F.; Roger, J.; Pons, J. N.; Bacri, J. C. Interaction of Anionic Superparamagnetic Nanoparticles with Cells: Kinetic Analyses of Membrane Adsorption and Subsequent Internalisation. *Langmuir* **2002**, *18*, 8148–8155.
33. Adolphi, N. L.; Huber, D. L.; Bryant, H. C.; Monson, T. C.; Fegan, D. L.; Lim, J.-K.; Trujillo, J. E.; Tessier, T. E.; Lovato, D. M.; Butler, K. S.; et al. Characterisation of Single-Core Magnetite Nanoparticles for Magnetic Imaging by SQUID Relaxometry. *Phys. Med. Biol.* **2010**, *55*, 5985–6003.
34. Lee, P. N.; O'Neill, J. A. The Effect Both of Time and Dose Applied on Tumour Incidence Rate in Benzopyrene Skin Painting Experiments. *Br. J. Cancer* **1971**, *25*, 759–770.
35. Newman, M. C.; McCloskey, J. T. Time-To-Event Analyses of Ecotoxicity Data. *Ecotoxicology* **1996**, *5*, 187–196.
36. Sanchez-Bayo, F. From Simple Toxicological Models to Prediction of Toxic Effects in Time. *Ecotoxicology* **2009**, *18*, 343–354.
37. Simon, S. M.; Schindler, M. Cell Biological Mechanisms of Multidrug Resistance in Tumors. *Proc. Natl. Acad. Sci. U.S.A.* **1994**, *91*, 3497–3504.
38. Jin, H.; Heller, D. A.; Strano, M. S. Single-Particle Tracking of Endocytosis and Exocytosis of Single-Walled Carbon Nanotubes in NIH-3T3 Cells. *Nano Lett.* **2008**, *8*, 1577–1585.
39. Brown, M. R.; Summers, H. D.; Rees, P.; Chappell, S. C.; Silvestre, O. F.; Khan, I. A.; Smith, P. J.; Errington, R. J. Long-Term Time Series Analysis of Quantum Dot Encoded Cells By Deconvolution of the Autofluorescence Signal. *Cytometry A* **2010**, *77A*, 925–932.
40. Dykens, J. A.; Will, Y. The Significance of Mitochondrial Toxicity Testing in Drug Development. *Drug Discovery Today* **2007**, *12*, 777–785.
41. Xia, T.; Kovochich, M.; Liong, M.; Zink, J. I.; Nel, A. E. Cationic Polystyrene Nanosphere Toxicity Depends on Cell-Specific Endocytic and Mitochondrial Injury Pathways. *ACS Nano* **2008**, *2*, 85–96.
42. Vander Heiden, M. G.; Cantley, L. C.; Thompson, C. B. Understanding the Warburg Effect: The Metabolic Requirements of Cell Proliferation. *Science* **2009**, *324*, 1029–1033.
43. Ferrari, M. Cancer Nanotechnology: Opportunities and Challenges. *Nat. Rev. Cancer* **2005**, *5*, 161–171.
44. Thybaud, V.; Aardema, M.; Clements, J.; Dearfield, K.; Galloway, S.; Hayashi, M.; Jacobson-Kram, D.; Kirkland, D.; MacGregor, J. T.; Marzin, D.; et al. Expert Working Group on Hazard Identification and Risk Assessment in Relation to *In Vitro* Testing. Strategy for Genotoxicity Testing: Hazard Identification and Risk Assessment in Relation To *In Vitro* Testing. *Mutat. Res.* **2007**, *627*, 41–58.
45. Majithia, R.; Patterson, J.; Bondos, S. E.; Meissner, K. E. On the Design of Composite Protein–Quantum Dot Biomaterials *via* Self-Assembly. *Biomacromolecules* **2011**, *12*, 3629–3637.